Korean J. Chem. Eng., 36(8), 1258-1266 (2019)
DOI: 10.1007/s11814-019-0324-9

pISSN: 0256-1115
eISSN: 1975-7220

Density functional theory study of NO_x adsorption on alkaline earth metal oxide and transition metal surfaces

Jae Yul Lim*,‡, Kyeounghak Kim,‡, Eui Yong Kim*,†, and Jeong Woo Han**,†**

*Department of Chemical Engineering, University of Seoul, Seoul 02504, Korea
**Department of Chemical Engineering, Pohang University of Science and Technology (POSTECH), Pohang, Gyeongbuk 37673, Korea
(*Received 14 March 2019 • accepted 12 June 2019*)

Abstract−Since the emissions of nitrogen oxides (NO_x) from automobiles cause air pollution, NO_x storage-reduction (NSR) catalyst has been used to convert the NO_x into harmless components such as N_2 through the reduction of NO_x. In this study, to provide fundamental understanding of key elementary steps of NSR, we established an extensive database for the adsorption properties of NO and NO_2 on a wide range of metal and metal oxide surfaces. Our results show that the amount of charge transfer between NO_x and surface is closely related to the molecular adsorption strength of NO_x, and it changes the molecular stability of NO_x on the surfaces by enlarging the inner bond length of N-O. Understanding the adsorption energy of the molecules or atoms that would participate in the reaction can be important to predict the ability of NO_x storage and conversion in NSR. This study provides a useful insight for designing metals or metal oxides for NSR catalyst.

Keywords: NO_x Adsorption, NO_x Storage-reduction (NSR), Alkaline Earth Metal Oxide, Transition Metal, Density Functional Theory (DFT)

INTRODUCTION

The diesel engine has been widely used as a major part of automobiles, but it is also a main source of emission of harmful gases such as NO_x, SO_x, and CO_x [1,2]. Owing to the increased interest in environmental issues, such as global climate change or air pollution, there is a great demand for reduction or purification of automotive exhaust gases [3]. The conventional way to remove those harmful gases from the automobile emission is to use three-way catalysts (TWC) [4-7]. However, the removal efficiency of NO_x through the TWC in a diesel engine under operating conditions is not easy to satisfy international regulations such as Euro 6 due to the excess oxygen in the exhaust gas [8,9]. As one of the ways to solve this problem, the NO_x storage-reduction (NSR) catalyst has been studied [10-13]. The NSR catalyst generally consists of precious or transition metals for NO_x conversion, alkaline earth oxides for NO_x storage, and metal oxides for their support. Although the exact mechanism of the NSR is still unclear [12], the commonly suggested NSR reaction mechanism at different fuel conditions is as follows [12,14-18]: at lean-burn cycles, NO is oxidized to NO_2 reacting with O_2 on the surfaces of transition metal catalysts, then it is stored into alkaline earth oxides in the form of nitrites or nitrates. At rich-burn cycles, however, nitrites or nitrates are released from alkaline earth metal oxides, and then it is reduced to N_2 on transition metal or precious metal surfaces.

In this sense, NO_x adsorption is a key elementary step in NSR reactions, regardless of reaction conditions. For these reasons, many theoretical papers have reported the adsorption of NO_x on alkaline earth metal oxides or transition metals. However, they have focused on only a specific group such as alkaline earth metal oxides [18,19] or transition metals [20]. Until now, thus, it has been hard to compare those results comprehensively due to the inconsistency of calculation tools or details.

Therefore, in this study, we investigated the adsorption geometry and energetics of NO and NO_2 on the surfaces of 4 alkaline metal oxides and 11 transition metals using the consistent framework of DFT calculations. Our results provide a fundamental understanding of interactions between NO_x and NSR catalysts at the atomic scale, and valuable insight to design the enhanced NSR catalyst.

COMPUTATIONAL METHODS

All density functional theory (DFT) calculations were carried out using the Vienna ab initio simulation package (VASP) [21,22], using generalized gradient approximation (GGA) [23] for the exchange and correlation functional based on Perdew-Burke-Ernzerhof (PBE). A plane-wave basis set with a cutoff energy of 400 eV was employed. Bader charge analysis was used for the charge calculations. In all slab model calculations, the atoms were relaxed using conjugate gradient-based optimization until the residual forces were less than 0.03 eV/Å. Dipole corrections were applied in all surface calculations.

For alkaline earth metal oxides of MgO, CaO, BaO, and SrO, rock-salt structure of (2×2) surface unit cells were used with a vacuum thickness of 15 Å. The DFT-optimized lattice constants of 4.25,

†To whom correspondence should be addressed.
E-mail: eykim@uos.ac.kr, jwhan@postech.ac.kr
‡J. Y. Lim and K. Kim contributed equally to this work.

4.82, 5.20, and 5.58 Å were used for MgO(001), CaO(001), BaO(001), and SrO(001), respectively, which are in good agreement with experimental results [24]. The Monkhorst-Pack grid of 6×6×1 *k*-points [25] was used. The bottom two layers were fixed in their bulk positions while the other upper three layers were fully relaxed. Gaussian smearing was used with a width of 0.05 eV to determine the partial occupancies.

For 11 transition metals, (3×3) surface unit cells were used with a vacuum thickness of 15 Å to describe the surface structure. The Monkhorst-Pack grid of 7×7×1 *k*-points was used. The bottom two layers were fixed in their bulk positions while the other upper three layers were fully relaxed. Methfessel-Paxton Fermi-level smearing was used with a width of 0.1 eV to determine the partial occupancies. We considered spin-polarization for the calculations of Fe(110), Co(0001) and Ni(111). For face-centered cubic (FCC) structures of Ag, Au, Cu, Pd, Pt, Ir, Rh and Ni, the (111) surfaces with DFT-optimized lattice constants of 4.14, 4.16, 3.62, 3.93, 3.96, 3.86, 3.82, and 3.51 Å were used respectively. For hexagonal close packed (HCP) structures, the (0001) surfaces with DFT-optimized lattice constants of a=2.71 Å and c=4.34 Å for Ru and a=2.45 Å, c=3.95 Å for Co were used, respectively. For body centered cubic (BCC) structure of Fe, the DFT-optimized lattice constant of 2.83 Å was used for Fe(110) surface [26]. The geometries of gas phase molecules were optimized in the large periodically repeated cubic boxes (approximately 20 Å on a side) using the Monkhorst-Pack grid of 12×12×12 *k*-points.

The adsorption energy (E_{ads}) is defined as follows:

$$E_{ads}=E_{total}-E_{surf}-E_{adsorbate},$$

where E_{total} is the total energy of NO_x adsorbed system, E_{surf} is the total energy of clean surface, and $E_{adsorbate}$ is the total energy of NO_x in gas phase. The charge transfer (Δq) between surface and adsorbate is defined as follows:

$$\Delta q=q_{NOx^*}-q_{NOx}$$

We used Bader charge analysis to obtain the amount of transferred charges by calculating the difference between total amount of chages in NO_x before (gas phase) and after molecular adsorption. Based on our definition, a positive value means that the charge transfer occurs from the surface to the NO_x.

RESULTS AND DISCUSSION

The optimized structures of NO and NO_2 in the gas phase are shown in Fig. 1. NO(g) showed a linear structure with the bond length of 1.17 Å between N and O atom while NO_2(g) was optimized to a bent structure with ∠O-N-O angle of 133.37° and N-O bond length of 1.21 Å. These optimized structures are in good agreement with previously reported bond lengths and angles of both NO (1.169 Å, 180°) and NO_2 (1.213 Å, 133.7°) [27].

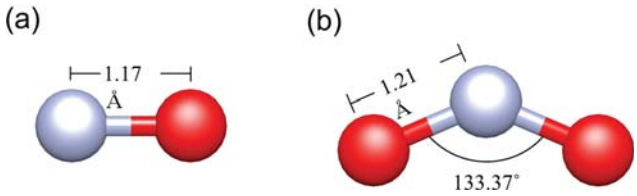

Fig. 1. Optimized structures of gas-phase (a) NO and (b) NO_2. The blue sphere represents nitrogen and the red sphere represents oxygen.

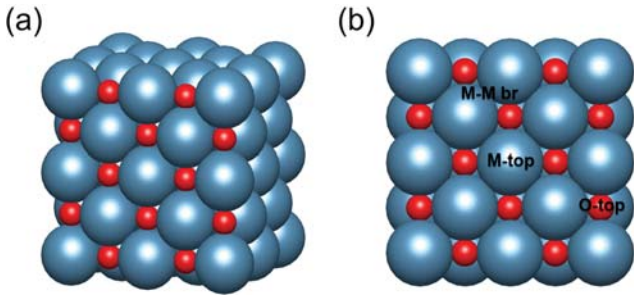

Fig. 2. (a) Side and (b) top views of surface structure of alkaline earth metal surface. The possible adsorption sites are marked in (b). The navy blue and red spheres represent the cation and oxygen, respectively.

1. NO Adsorption Properties on Alkaline Earth Metal Oxides Group

The crystal structure of alkaline earth metal oxide is the rock salt, and there are three possible adsorption sites of M-top, M-M bridge, and O-top for the adsorbates on MgO(001), CaO(001), SrO(001), and BaO(001), which have been known as the most stable surface [28] (Fig. 2). M-top site is the top site of cation M, M-M bridge site is a two-fold site between two surface cations, and the O-top site is the top site of surface lattice oxygen atom, respectively.

Table 1 shows the detailed information for the adsorption structures of NO on the alkaline earth metal oxide surfaces, and the optimized structures are shown in Fig. 4(a)-(d). In the case of MgO(001), NO physisorbed at the Mg-Mg bridge site on the surface with an weak adsorption energy of −0.15 eV. N-down adsorption configuration of NO was more stable than O-down one for all alkaline earth metal oxide surfaces [27]. From the long distance of 2.46 Å between absorbed NO and MgO(001), it is reasonably thought that NO is physisorbed on MgO(001), which is in good

Table 1. Bond lengths between NO and surface ($d_{N(NO)-sur}$), inner bond lengths of N-O in adsorbed NO ($d_{N-O(NO)}$), bond angles of NO with alkaline earth metal surfaces, adsorption sites, amount of charge transfer, and adsorption energies on alkaline earth metal surfaces

NO	$d_{N(NO)-sur}$ (Å)	$d_{N-O(NO)}$ (Å)	∠NOA_{sur} (deg)	Site	Q (e^-)	E_{ads} (eV)
MgO(001)	2.46	1.17	117.22	M-Br	−0.24	−0.15
CaO(001)	1.63	1.30	108.05	O-top	−0.66	−0.68
SrO(001)	1.58	1.31	108.90	O-top	−0.67	−1.14
BaO(001)	1.57	1.32	110.02	O-top	−0.70	−1.46

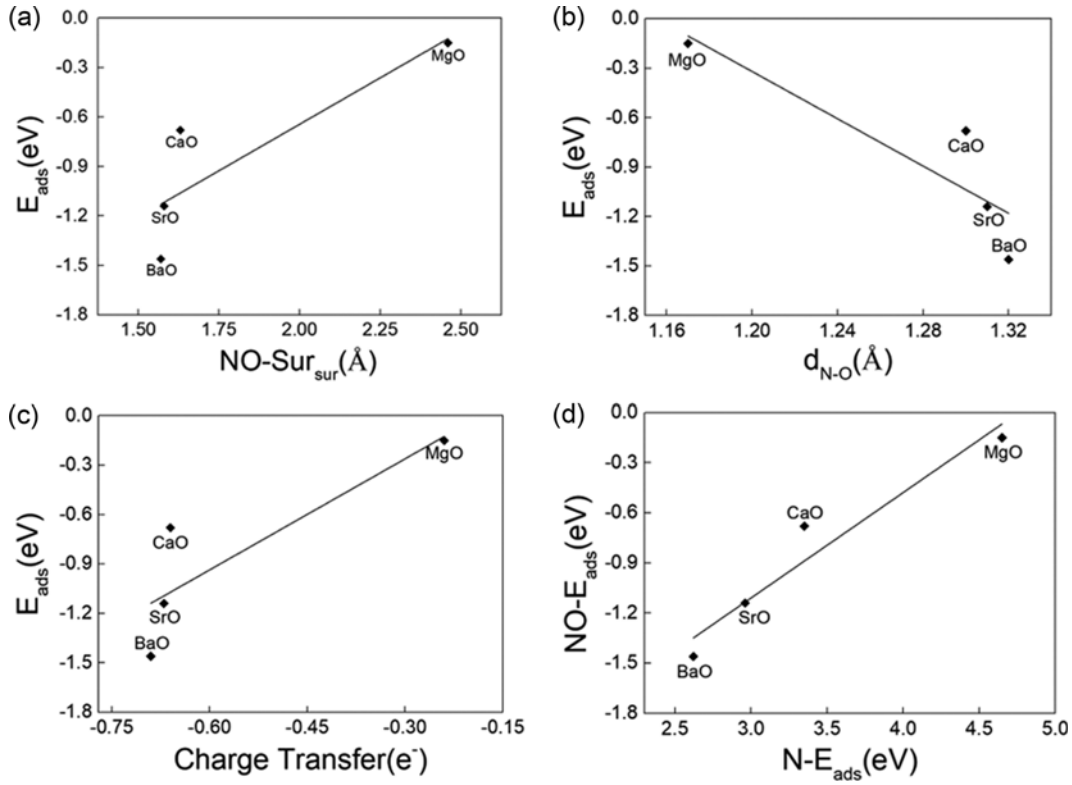

Fig. 3. Linear relationship of NO adsorption energy with (a) bond length between an N atom in adsorbed NO and the surface ($d_{N\text{-}sur}$), (b) inner bond length of N-O in adsorbed NO ($d_{N\text{-}O}$), and (c) amount of charge transfer. (d) Scaling relationship between the adsorption energies of NO and N on alkaline earth metal surfaces.

agreement with other theoretical [27,29,30] and experimental results [31]. The bond length between N and O in the adsorbed state (1.17 Å), quite similar to that in gas phase NO(g) (1.17 Å), also supports the physisorption characteristic (Table 1). On the contrary to MgO(001), NO chemisorbed at the O-top site of other alkaline earth metal oxide surfaces, CaO(001), SrO(001), and BaO(001), with much higher adsorption energies of −0.68, −1.14, and −1.46 eV, respectively. In addition, the N-O bond length in the adsorbed NO was also evidently elongated on CaO(001), SrO(001), and BaO(001) from 1.17 Å (N-O in NO(g)) to 1.30 Å, 1.31 Å, and 1.32 Å, respectively (Table 1 and Fig. 3(b)). This implies the strong interaction of NO with CaO(001), SrO(001), and BaO(001).

As shown in Fig. 3(a), the bond length between N in the adsorbed NO and surface atoms ($d_{N\text{-}sur}$) increased with decreasing the adsorption strength, whereas that of N-O decreased with decreasing the adsorption strength. Since the strong interaction is attributed to the large transfer of charges between surface and adsorbate, the amount of charge transfer from surface to NO has a linear relationship with its adsorption energy (Fig. 3(c)). The larger amount of charge transfer from surface to NO results in stronger adsorption strength. This leads to a shorter adsorption distance between NO and the surface, as well as the weaker inner bond strength of the adsorbed NO by increasing the charges in the π antibonding orbital of the NO molecule [29]. However, regardless of the type of cation in alkaline earth metal oxide, NO shows tilted adsorption configurations due to the interaction between extra unpaired electron of the NO and the surface cation [28].

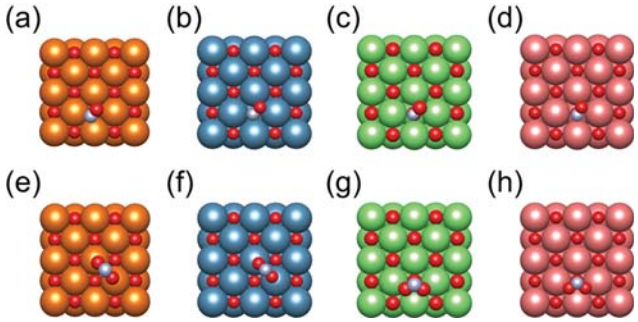

Fig. 4. Top views of the most stable adsorption structures of (a)-(d) NO and (e)-(h) NO_2 on alkaline earth metal oxides of ((a) and (e)) MgO(001), ((b) and (f)) CaO(001), ((c) and (g)) SrO(001), and ((d) and (h)) BaO(001).

Since NO adsorbs on the surfaces of alkaline earth metal oxide through N atom (Fig. 4(a)-(d)), its adsorption energy may be reasonably estimated by using only the adsorption energy of N on the surfaces, which directly participates in molecular adsorption [32]. Fig. 3(d) confirms the linear relationship with an equation of E_{ads} (NO)= $0.58E_{ads}$ (N)−2.85 on the surfaces of alkaline earth metal oxide within small mean absolute error (MAE) of 0.11 eV.

2. NO_2 Adsorption Properties on Alkaline Earth Metal Oxides Group

Contrary to the NO adsorption, NO_2 preferentially adsorbed at the cation of alkaline earth metal oxide surface through two O atoms

Table 2. Bond lengths between NO_2 and surface ($d_{N(NO2)\text{-}sur}$), average inner bond lengths of two N-O in adsorbed NO_2 ($d_{N\text{-}O(NO2)}$), inner bond angles of NO_2, adsorption sites, amount of charge transfer, and adsorption energies on alkaline earth metal surfaces

NO_2	$d_{N(NO2)\text{-}sur}$ (Å)	$d_{N\text{-}O(NO2)}$ (Å)	∠ONO (deg)	Site	Q (e^-)	E_{ads} (eV)
MgO(001)	2.73	1.24	123.65	t-b-t	−0.40	−0.57
CaO(001)	2.67	1.26	119.79	t-b-t	−0.62	−0.94
SrO(001)	2.62	1.27	115.33	b-o-b	−0.83	−1.19
BaO(001)	2.51	1.28	114.49	b-o-b	−0.90	−1.63

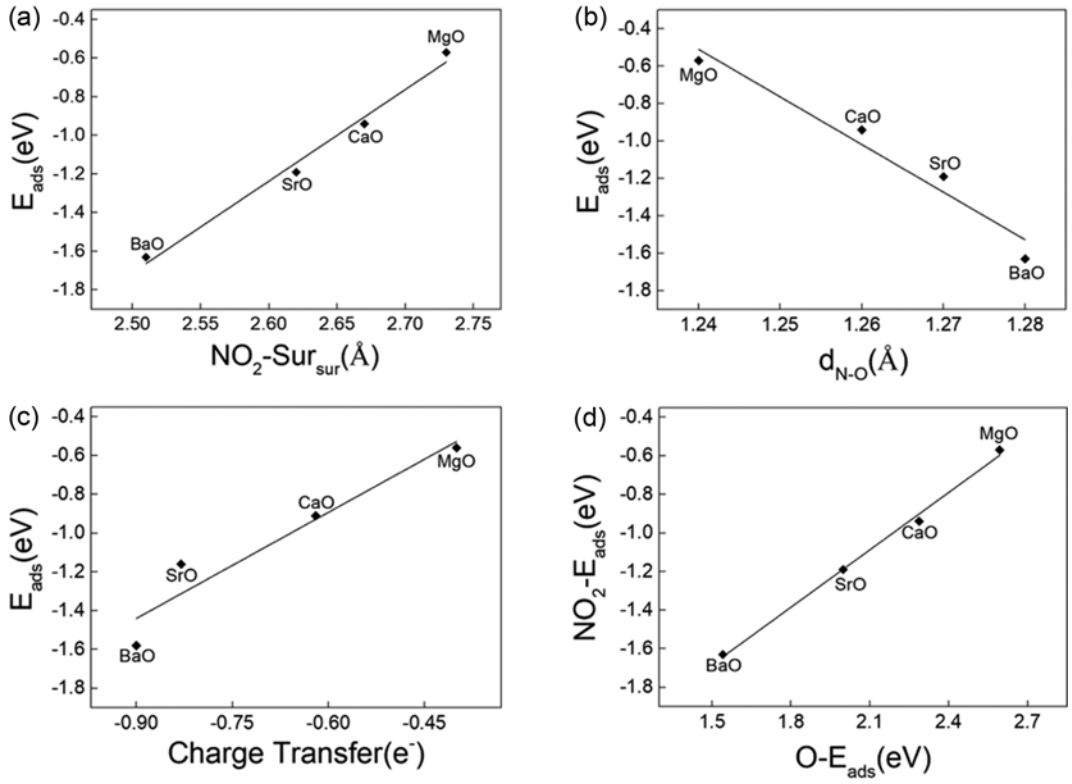

Fig. 5. Linear relationship of NO_2 adsorption energy with (a) bond length between NO_2 and surface ($d_{N(NO2)\text{-}sur}$), (b) average inner bond length of two N-O in adsorbed NO_2 ($d_{N\text{-}O(NO2)}$), and (c) amount of charge transfer. (d) Scaling relationship between the adsorption energies of NO_2 and N on alkaline earth metal surfaces.

in NO_2, which is in good agreement with the other works [29] (Fig. 4(e)-(h)). Schneider also reported that Lewis-base-like O-down adsorption was more stable than Lewis-acid-like N-down adsorption on MgO(001) [27]. The NO_2 adsorption energies were in order of MgO (−0.57 eV)<CaO (−0.94 eV)<SrO (−1.19eV)<BaO (−1.63 eV). Similar to the NO adsorption, the average N-O bond lengths in the adsorbed NO_2 were also evidently enlarged from 1.21 to 1.24-1.28 Å as the adsorption strength increased (Table 2 and Fig. 5(b)). NO_2 chemisorbed at MgO(001) with higher adsorption energy of −0.57 eV than that of NO (−0.15 eV). The average bond lengths between N in NO_2 and the surfaces also decreased from 2.73 to 2.51 Å as the adsorption strength increased (Table 2 and Fig. 5(a)). This implies stronger interaction of NO_2 with surface atoms results in weaker inner bond strength between N-O in the adsorbed NO.

The charge transfer also has a linear relationship to the adsorption energy of NO_2 (Fig. 5(c)). The adsorption strength became stronger as the amount of transferred charge from surface to the NO_2 increased (Fig. 5(c)). Thus, the amount of charge transfer between alkaline earth metal oxides and NO_2 also followed the order of MgO<CaO<SrO<BaO. Since NO_2 chemisorbed at the surface by forming two covalent bonds between two O atoms in the adsorbed NO_2 and surface cations [29], larger charge transfer resulted in the stronger adsorption strength of NO_2 on alkaline earth metal oxide surfaces. In addition, an N atom in NO_2 prefers to make a bond to the surface lattice oxygen by decreasing the distance between N_{NO2}-O_{latt}.

For NO_2 adsorption, two O atoms in NO_2 directly participated in molecular adsorption (Fig. 4(e)-(h)). Therefore, the adsorption energies of O and NO_2 on the surfaces of alkaline earth metal oxide showed a linear relationship under the equation of E_{ads} (NO_2)= $1.00E_{ads}$ (O)− 3.16 within small MAE of 0.02 eV (Fig. 5(d)).

3. NO Adsorption Properties on Transition Metals

For transition metal group, 11 candidate metals are classified into three surfaces types of (111), (0001), and (110). We investigated all possible adsorption sites of top, bridge, hcp-hollow, and

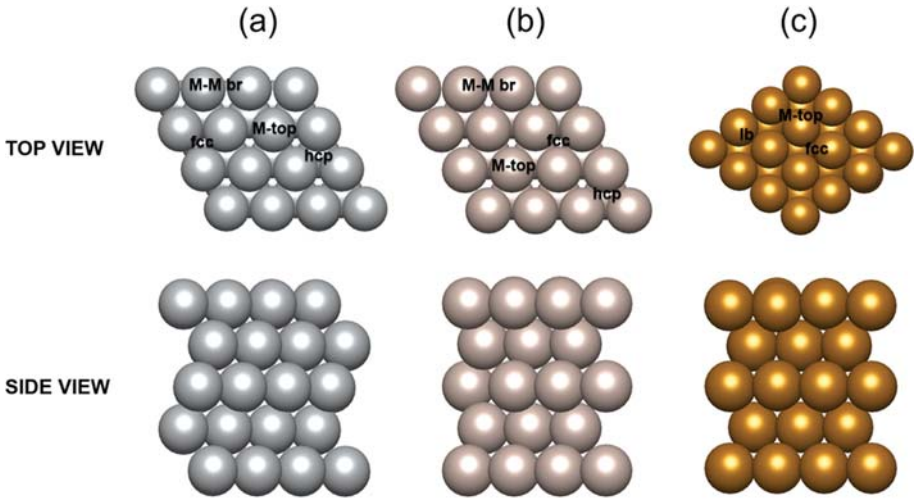

Fig. 6. (a)-(c) Top and side view structures of transition metals with the possible adsorption sites on (111), (0001), and (110) surfaces.

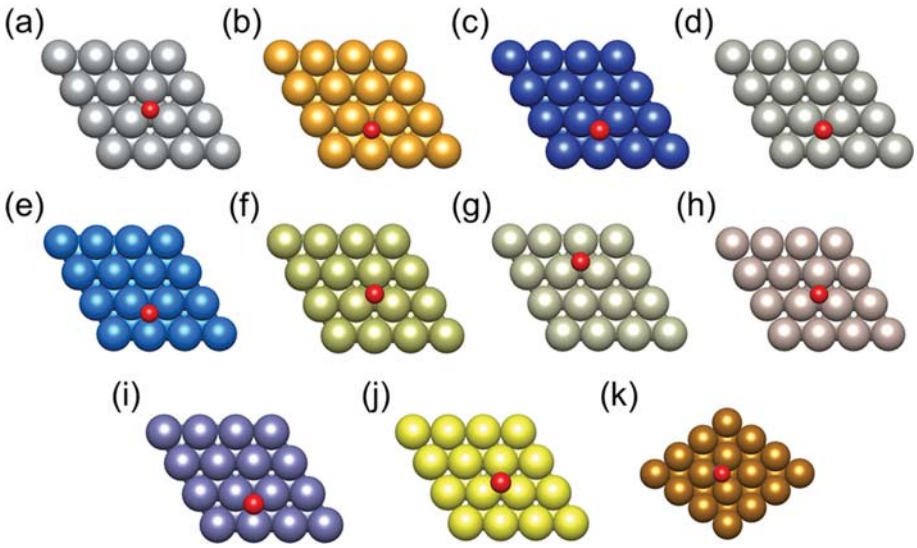

Fig. 7. Top views of the optimized NO adsorbed structures on the transition metal surfaces of (a) Ag(111), (b) Au(111), (c) Cu(111), (d) Pd(111), (e) Pt(111), (f) Ir(111), (g) Rh(111), (h) Ru(0001), (i) Ni(111), (j) Co(0001), and (k) Fe(110)

Table 3. Bond lengths between NO and surface ($d_{N(NO)\text{-}sur}$), inner bond lengths of N-O in adsorbed NO ($d_{N\text{-}O(NO)}$), bond angles of NO with transition metal surfaces, adsorption sites, amount of charge transfer, and adsorption energies on transition metal surfaces

NO	$d_{N(NO)\text{-}sur}$ (Å)	$d_{N\text{-}O(NO)}$ (Å)	∠NOA_{sur} (deg)	Site	Q (e^-)	E_{ads} (eV)
Ag(111)	2.15	1.21	120.26	fcc	−0.37	−0.68
Au(111)	2.02	1.20	126.49	fcc	−0.27	−0.57
Cu(111)	1.96	1.22	130.20	fcc	−0.50	−1.49
Pd(111)	1.87	1.21	125.92	fcc	−0.34	−2.65
Pt(111)	1.93	1.21	126.82	hcp	−0.38	−2.24
Ir(111)	1.99	1.22	129.68	hcp	−0.49	−2.39
Rh(111)	1.95	1.22	128.70	hcp	−0.45	−2.86
Ru(0001)	1.93	1.24	127.83	fcc	−0.64	−3.02
Ni(111)	1.82	1.22	129.78	fcc/hcp	−0.56	−2.82
Co(0001)	2.03	1.23	136.74	hcp	−0.51	−2.65
Fe(110)	1.85	1.24	127.15	fcc	−0.68	−3.20

fcc-hollow that are symmetrically nonequivalent for NO and NO_2 adsorptions (Fig. 6). NO vertically adsorbed at fcc- or hcp-hollow site of transition metal surfaces with an N-down configuration (Fig. 7(a)-(j)) [20]. Only Fe(110) showed a little tilted adsorption configuration (Fig. 7(k)). The detailed structural information for molecular adsorption of NO is shown in Table 3. For FCC structures, NO was the most stable at the fcc-hollow site of Ag(111), Au(111), Cu(111), and Pd(111) with the adsorption energies of −0.68, −0.57, −1.49, and −2.65 eV, respectively. For Pt(111), Ir(111), Rh(111), and Ni(111), however, hcp-hollow site was the most stable with the adsorption energies of −2.24, −2.39, −2.86, and −2.82 eV, respectively. For HCP structures of Ru(0001) and Co(0001), NO prefer-

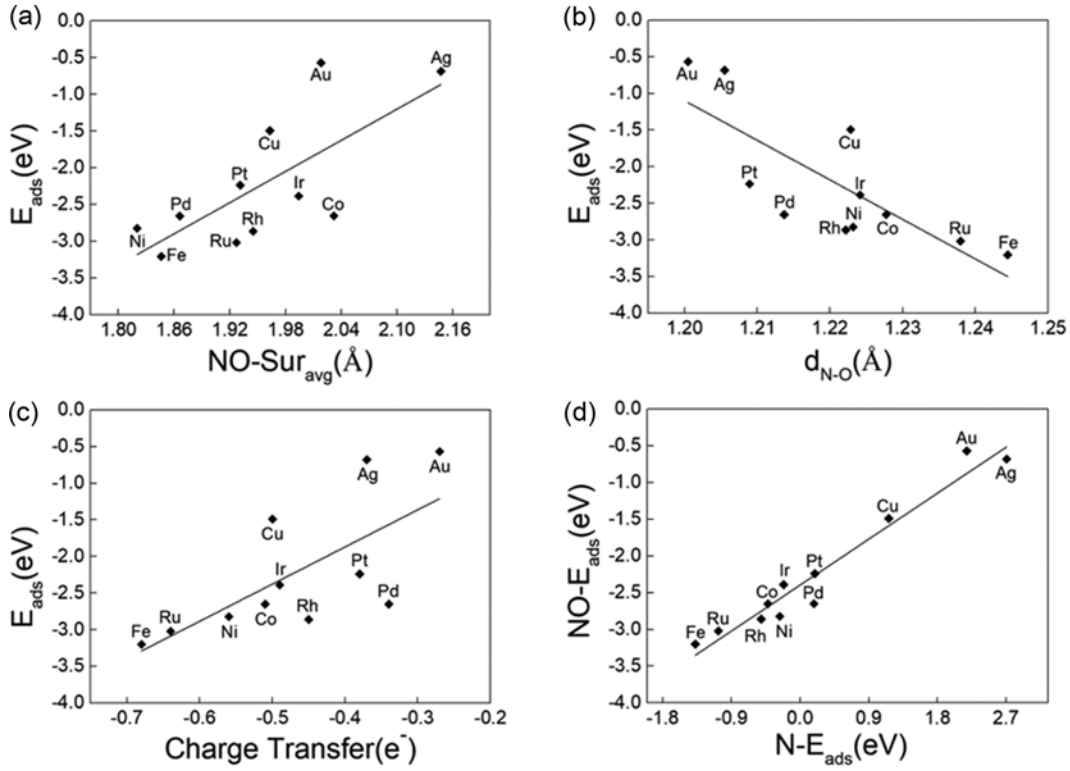

Fig. 8. Linear relationship of NO adsorption energy with (a) bond length between an N atom in adsorbed NO and the surface ($d_{N\text{-}sur}$), (b) inner bond length of N-O in adsorbed NO ($d_{N\text{-}O}$), and (c) amount of charge transfer. (d) Scaling relationship between the adsorption energies of NO and N on transition metal surfaces.

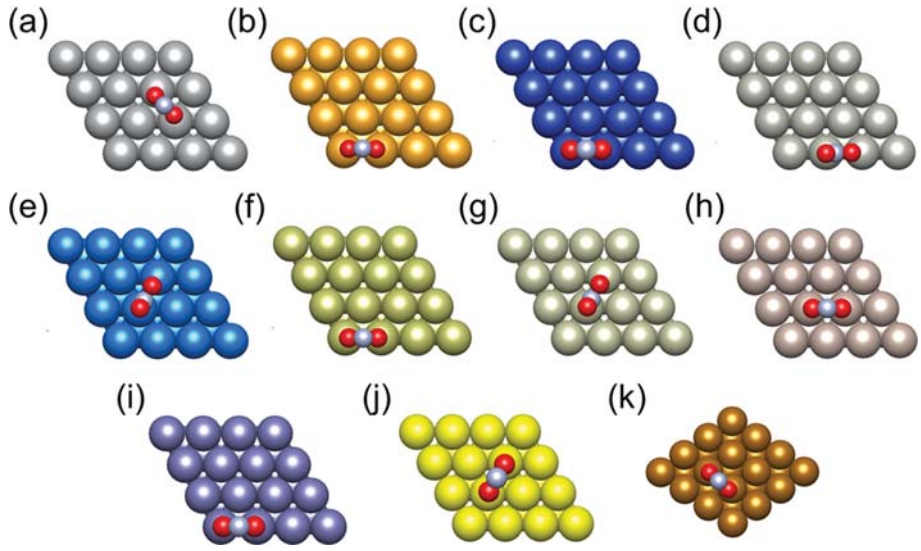

Fig. 9. Top views of the optimized NO_2 adsorbed structures on the transition metal surfaces of (a) Ag(111), (b) Au(111), (c) Cu(111), (d) Pd(111), (e) Pt(111), (f) Ir(111), (g) Rh(111), (h) Ru(0001), (i) Ni(111), (j) Co(0001), and (k) Fe(110).

entially adsorbed at the fcc-hollow and hcp-hollow sites with the adsorption energies of −3.02 and −2.65 eV, respectively. The BCC structure of Fe(110) showed a fcc-hollow site as the most stable site for NO adsorption with the adsorption energy of −3.20 eV.

To investigate the change of molecular structure of NO upon its adsorption onto transition metal surfaces, we examined the distance between transition metal surface and N atom in the adsorbed NO, similarly to the case of alkaline earth metal oxide. As the adsorption energy increased, a longer N-O bond length in the adsorbed NO as well as shorter bond length between an N atom of the adsorbed NO and surface atoms ($d_{N\text{-}sur}$) was observed. The charge transfer occurred from the transition metal surface to NO upon the molecular adsorption, and the amount of charge transfer showed a linear relationship to the adsorption energy. The linear relationship between the adsorption energies of NO and N with an equation of E_{ads} (NO)=0.63E_{ads} (N)−2.44 was also found on the transition metal surfaces within small MAE of 0.16 eV (Fig. 8(d)).

4. NO_2 Adsorption Properties on Transition Metals

In NSR at lean-fuel condition, NO_2 is the product of NO oxidation. After the conversion of NO into NO_2, it should be easily de-

Table 4. Bond lengths between NO_2 and surface ($d_{N(NO2)\text{-}sur}$), average inner bond lengths of two N-O in adsorbed NO_2 ($d_{N\text{-}O(NO2)}$), inner bond angles of NO_2, adsorption sites, amount of charge transfer, and adsorption energies on transition metal surfaces

NO_2	$d_{N(NO2)\text{-}sur}$ (Å)	$d_{N\text{-}O(NO2)}$ (Å)	∠ONO (deg)	Site	Q (e^-)	E_{ads} (eV)
Ag(111)	2.56	1.26	150.54	t-b-t	−0.54	−1.43
Au(111)	2.58	1.25	123.25	t-b-t	−0.37	−1.01
Cu(111)	2.36	1.27	118.89	t-b-t	−0.58	−1.72
Pd(111)	2.35	1.26	120.48	t-b-t	−0.39	−1.65
Pt(111)	2.36	1.27	118.92	t-b-t	−0.35	−1.67
Ir(111)	2.37	1.27	120.15	t-b-t	−0.46	−1.98
Rh(111)	2.36	1.27	118.39	t-b-t	−0.46	−2.21
Ru(0001)	2.35	1.28	117.54	t-b-t	−0.59	−2.40
Ni(111)	2.29	1.27	118.26	t-b-t	−0.52	−1.97
Co(0001)	2.32	1.28	117.76	t-b-t	−0.55	−1.98
Fe(110)	2.26	1.29	115.01	t-lb-t	−0.62	−2.43

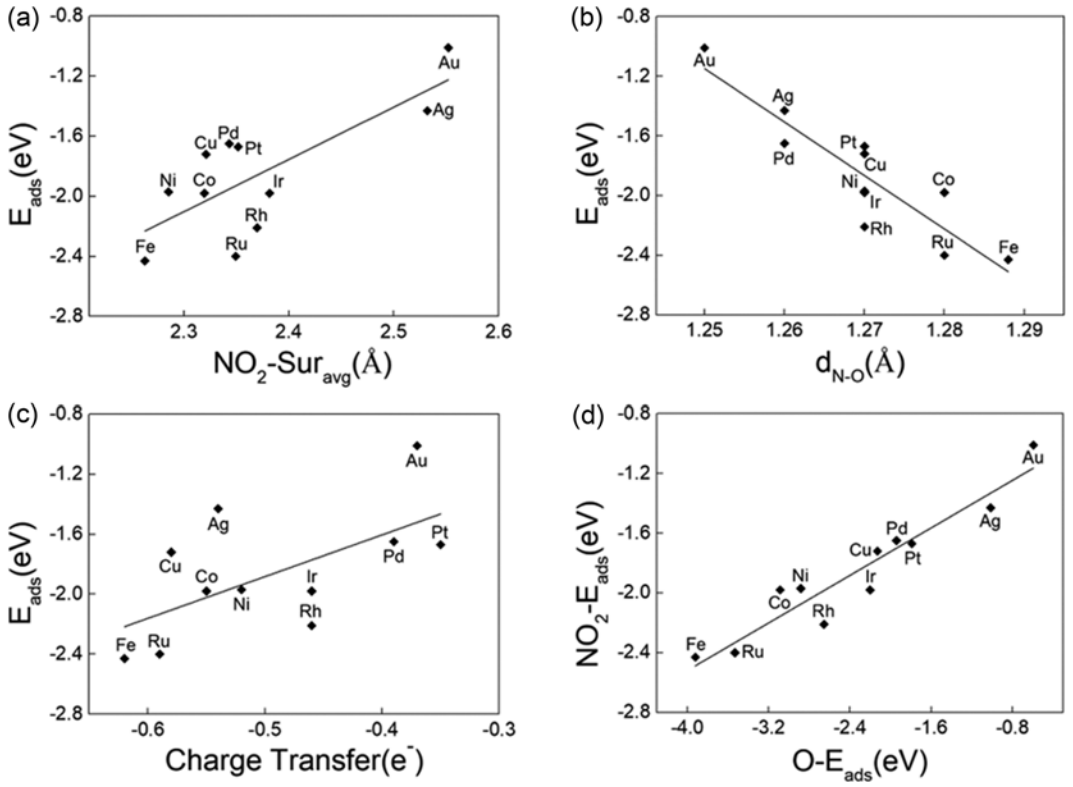

Fig. 10. Linear relationship of NO_2 adsorption energy with (a) bond length between NO_2 and surface ($d_{N(NO2)\text{-}sur}$), (b) average inner bond length of two N-O in adsorbed NO_2 ($d_{N\text{-}O(NO2)}$), and (c) amount of charge transfer. (d) Scaling relationship between the adsorption energies of NO_2 and N on transition metal surfaces.

sorbed from the transition metal surfaces. NO_2 preferentially adsorbed on the surfaces through two O atoms in NO_2 (oxygen-down adsorption configuration as shown in Fig. 9), which is in good agreement with previous reports [20]. As the adsorption energy increased, the distance between NO_2 and transition metal surface decreased, while the average bond length between N-O in NO_2 increased. This tendency is similar to that in alkaline earth metal oxide surfaces. Charge transfer also occurred from transition metal surface to NO_2, and a linear relationship between the amount of charge transfer and adsorption energy was observed. Because of the similar adsorption configurations of NO_2 on transition metals (Fig. 9) to those on alkaline earth meal oxides (Fig. 4(e)-(h)), the adsorption energy of NO_2 can also be estimated only by that of O (Fig. 10(d)) with an equation of E_{ads} (NO)=0.40E_{ads} (O)−0.93 within very small MAE of 0.11 eV.

5. Application of Our Database to Predict the Activity of NSR Catalyst

In this section, we discuss how our results can be applied to predict the activity of NSR on alkaline earth metal oxide and transition metal surfaces. The role of these surfaces in NSR is as follows: (1) adsorption of NO, (2) conversion of NO to NO_2, and (3) NO_2 desorption to store it into alkaline earth metal oxide. As a descriptor to predict the catalytic activity of NO oxidation on transition metal surfaces, Song et al. reported a linear relationship between the reaction barrier from NO to NO_2 and the sum of adsorption energies of NO and O [20]. This indicates that the elementary steps of (1) and (2) are not independent, and thus more negative adsorption energy of NO represents the easier adsorption as well as the easier conversion of NO to NO_2. Therefore, we can reasonably suggest the sum of energies for NO adsorption (related to the elementary steps (1) and (2)) and NO_2 desorption (elementary step (3)), E_{ads} (NO-NO_2)=E_{ads} (NO)+(−E_{ads} (NO_2)), as a descriptor to predict the NSR activity of transition metal catalysts (Fig. 11(a)). The more negative value of E_{ads} (NO-NO_2) represents the easier ability of both NO adsorption and NO_2 desorption. Our results show that precious metals such as Pd, Rh, Ni, and Ru have more negative E_{ads} (NO-NO_2) than other transition metal candidates, which is in good agreement with previous experimental reports [33].

We previously demonstrated that the adsorption strength can be optimized by introducing binary transition metal alloys, and consequently, some of alloy candidates could show even higher catalytic activity for CO oxidation than pure metals [26]. This strategy might be one way to optimize the catalytic activity of transition metal in NSR. In addition to alloys, tuning the size and morphology of transition metal catalyst can change the activity of NO oxidation [20]. For example, stepped surfaces, which are the key characteristic of small size of nanoparticles, may exhibit lower energies of reaction barrier than terrace surfaces [20]. In this regard, Xue et al. showed that catalytic turnover frequencies of NO to NO_2 per exposed Pt atom on silica depend on Pt particle size in the range of 1.3-21 nm [34]. Villani et al. also reported that the reaction rate for NO oxidation per exposed Pt atom increases with increasing Pt particle size up to 20 nm because very fine Pt particles smaller than 5 nm in zeolite micropores could be electron-deficient as a result of electron transfer to the zeolite [35]. Although we focused on the interaction between NO_x and the most stable surfaces of the catalysts in this study, the optimization of the nanoparticle size and morphology of catalysts is also important and should be further studied in detail.

For alkaline earth metal oxide, the adsorption strengths of NO_2 were in order of BaO>SrO>CaO>>MgO (Fig. 11(b)). For this reason, BaO has been widely used for the NO_2 adsorbent in NSR [19]. Its redox ability may be further increased by doping with transition metals by changing the bond strength between surface cations and oxygen atoms [29,36,37]. In this sense, Añez et al. demonstrated that doping with transition metal atoms such as V, Fe, and Ni, which have higher ability of charge transfer from surface to the NO_2 in the subsurface of MgO(100) and BaO(001) than the host atoms, enhanced the adsorption strength of NO_2 [29].

Although we limited our focus particularly to molecular adsorption for NSR in this study, the elementary steps of NO_2 reduction and O_2 dissociation should also be investigated to precisely design the enhanced catalysts of NSR. In addition to the activity of catalysts, stability, selectivity, cost of catalyst will be also important factors in commercializing the improved NSR catalysts.

CONCLUSION

We performed DFT calculations to explore the adsorption properties of NO and NO_2 on a wide range of metal and metal oxide surfaces. The adsorption energetics are closely related to charge transfer from surface to the adsorbate, which affects molecular structure of the adsorbed NO_x. The scaling relationships between the adsorption energies of NO and N or NO_2 and O were found regardless

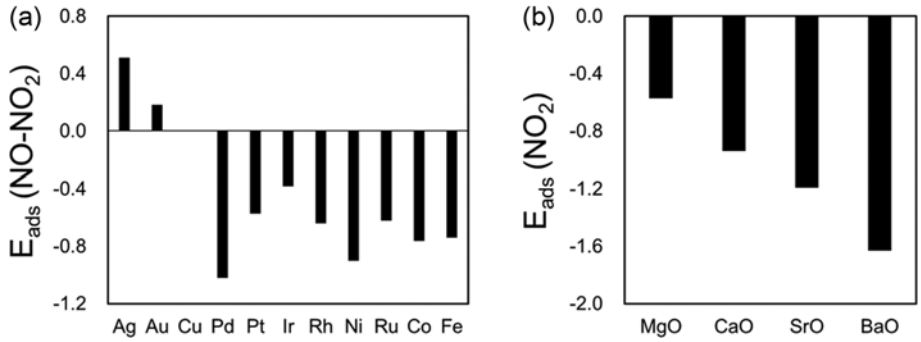

Fig. 11. (a) Difference in the adsorption energies (in eV) between NO and NO_2 on various transition metal surfaces. (b) Adsorption energies of NO_2 on alkaline earth metal surfaces.

of surface type, which would make it easier to estimate the adsorption energy of NO_x. Based on our results, we suggest the sum of NO adsorption and NO_2 desorption energy on transition metal surface as a descriptor for screening the highly active NSR. For alkaline earth metal oxides, the adsorption strength of NO_2, which would be stored in them, was in order of BaO>SrO>CaO>MgO.

ACKNOWLEDGEMENTS

This study was supported by the Basic Science Research Program (NRF2016R1A5A1009592 and NRF-2018R1A2B2002875) through the National Research Foundation of Korea (NRF) grant funded by the Korea government (MSIT) for Jeong Woo Han. Also, this work was supported by the 2016 Research Fund of the University of Seoul for Eui Yong Kim.

REFERENCES

1. F. Klingstedt, K. Arve, K. Eränen and D. Y. Murzin, *Acc. Chem. Res.*, **39**, 273 (2006).
2. S. Gallardo, T. Aida and H. Niiyama, *Korean J. Chem. Eng.*, **15**, 480 (1998).
3. L. Zhu, Z. Zhong, H. Yang, C. Wang and L. Wang, *Korean J. Chem. Eng.*, **34**, 1229 (2017).
4. D. N. Belton and K. C. Taylor, *Curr. Opin. Solid State Mater. Sci.*, **4**, 97 (1999).
5. K. C. Taylor, *Cat. Rev.*, **35**, 457 (1993).
6. R. M. Heck and R. J. Farrauto, *Appl. Catal. A-Gen.*, **221**, 443 (2001).
7. J. Wang, H. Chen, Z. Hu, M. Yao and Y. Li, *Cat. Rev.*, **57**, 79 (2015).
8. P. Granger and V. I. Parvulescu, *Chem. Rev.*, **111**, 3155 (2011).
9. H. Feng, C. Wang and Y. Huang, *Korean J. Chem. Eng.*, **34**, 2832 (2017).
10. W. S. Epling, L. E. Campbell, A. Yezerets, N. W. Currier and J. E. Parks, *Cat. Rev.*, **46**, 163 (2004).
11. Z. Liu and S. I. Woo, *Cat. Rev.*, **48**, 43 (2006).
12. S. Roy and A. Baiker, *Chem. Rev.*, **109**, 4054 (2009).
13. H. Cheng, G. Chen, S. Wang, D. Wu, Y. Zhang and H. Li, *Korean J. Chem. Eng.*, **21**, 595 (2004).
14. N. Takahashi, H. Shinjoh, T. Iijima, T. Suzuki, K. Yamazaki, K. Yokota, H. Suzuki, N. Miyoshi, S.-i. Matsumoto, T. Tanizawa, T. Tanaka, S.-s. Tateishi and K. Kasahara, *Catal. Today*, **27**, 63 (1996).
15. S. i. Matsumoto, *Catal. Today*, **29**, 43 (1996).
16. W. Bögner, M. Krämer, B. Krutzsch, S. Pischinger, D. Voigtländer, G. Wenninger, F. Wirbeleit, M. S. Brogan, R. J. Brisley and D. E. Webster, *Appl. Catal. B-Environ.*, **7**, 153 (1995).
17. E. Fridell, M. Skoglundh, B. Westerberg, S. Johansson and G. Smedler, *J. Catal.*, **183**, 196 (1999).
18. N.-X. Lu, J.-C. Tao and X. Xu, *Theor. Chem. Acc.*, **133**, 1565 (2014).
19. P. Broqvist, H. Grönbeck, E. Fridell and I. Panas, *J. Phys. Chem. B*, **108**, 3523 (2004).
20. Y. Song and L. C. Grabow, *Ind. Eng. Chem. Res.*, **57**, 12715 (2018).
21. G. Kresse and J. Furthmüller, *Phys. Rev. B.*, **54**, 11169 (1996).
22. G. Kresse and J. Furthmüller, *Comput. Mater. Sci.*, **6**, 15 (1996).
23. J. P. Perdew, K. Burke and M. Ernzerhof, *Phys. Rev. Lett.*, **77**, 3865 (1996).
24. R. W. G. Wyckoff, *Crystal structures - volume 1*, Interscience Publishers, New York (1963).
25. H. J. Monkhorst and J. D. Pack, *Phys. Rev. B.*, **13**, 5188 (1976).
26. J. Ko, H. Kwon, H. Kang, B.-K. Kim and J. W. Han, *Phys. Chem. Chem. Phys.*, **17**, 3123 (2015).
27. W. F. Schneider, *J. Phys. Chem. B*, **108**, 273 (2004).
28. M. Bajdich, J. K. Nørskov and A. Vojvodic, *Phys. Rev. B.*, **91**, 155401 (2015).
29. R. Añez, A. Sierraalta and L. J. D. Soto, *Appl. Surf. Sci.*, **404**, 216 (2017).
30. W. F. Schneider, K. C. Hass, M. Miletic and J. L. Gland, *J. Phys. Chem. B*, **106**, 7405 (2002).
31. R. Wichtendahl, M. Rodriguez-Rodrigo, U. Härtel, H. Kuhlenbeck and H.-J. Freund, *Phys. Status Solidi A*, **173**, 93 (1999).
32. K. Kim and J. W. Han, *Phys. Chem. Chem. Phys.*, **18**, 27775 (2016).
33. H. Abdulhamid, E. Fridell and M. Skoglundh, *Appl. Catal. B-Environ.*, **62**, 319 (2006).
34. E. Xue, K. Seshan and J. R. H. Ross, *Appl. Catal. B-Environ.*, **11**, 65 (1996).
35. K. Villani, W. Vermandel, K. Smets, D. Liang, G. Van Tendeloo and J. A. Martens, *Environ. Sci. Technol.*, **40**, 2727 (2006).
36. K. Kim, J. D. Yoo, S. Lee, M. Bae, J. Bae, W. Jung and J. W. Han, *ACS Appl. Mater. Interfaces*, **9**, 15449 (2017).
37. K. Kim and J. W. Han, *Catal. Today*, **293-294**, 82 (2017).